A PREDICTION MODEL FOR LIFT-FAN SIMULATOR PERFORMANCE

By

JOSEPH ALFRED YUSKA

A thesis submitted in partial fulfillment of the requirements

for the Degree of Master of Science

Examining Committee:

Assistant Professor, C. Jain, Chairman

~~Professor, C.~~ J. Kishel

Associate Professor, E. N. Poulos

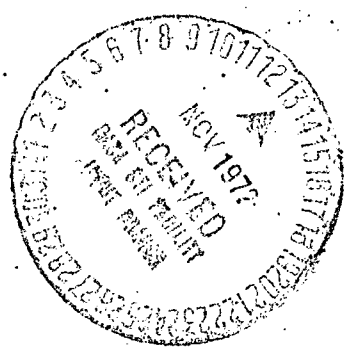

Department of Industrial Engineering

THE CLEVELAND STATE UNIVERSITY

August 1972

A PREDICTION MODEL FOR LIFT-FAN SIMULATOR PERFORMANCE

By

Joseph A. Yuska

Advisor: Dr. Chittaranjan Jain

ABSTRACT

In this report the performance characteristics of a model VTOL lift-fan simulator installed in a two-dimensional wing are presented. The lift-fan simulator consisted of a 15-inch diameter fan driven by a turbine contained in the fan hub. The performance of the lift-fan simulator was measured in two ways: (1) the calculated momentum thrust of the fan and turbine (total thrust loading), and (2) the axial-force measured on a load cell force balance (axial-force loading). Tests were conducted over a wide range of crossflow velocities, corrected tip speeds, and wing angle of attack.

The objective of this thesis work was to develop a prediction modeling technique to help in analyzing the performance characteristics of lift-fan simulators. A multiple linear regression analysis technique is presented which calculates prediction model equations for the dependent variables: total thrust loading and the axial-force loading as a function of the independent variables: crossflow velocity, corrected tip speed, and wing angle of attack. The results of the regression analysis show that there was a significant correlation for the two loading parameters as a function of the

independent variables. The results also showed that there is a significant correlation for the total thrust loading as a function of the axial-force loading.

The test results showed that the effect of increasing crossflow velocity is not the same for total thrust loading as for axial-force loading. The multiple linear regression analysis was used to determine a significant correlation for the difference between the two loading parameters for the same independent variables. Crossflow velocity was found to be the most significant variable in the force-loading difference correlation equation.

The results of this work indicate that this prediction modeling technique could be valuable in designing and analyzing lift-fan simulator tests. It could be used to reduce the amount of instrumentation required and to reduce the number of test runs required to define the performance characteristics of lift-fan simulators. The use of this technique could reduce the cost of building and testing lift-fan simulators.

ACKNOWLEDGEMENTS

The author is particularly indebted to Dr. C. Jain, thesis advisor, for his constant advice and guidance throughout this undertaking.

The author also wishes to express his graditude to the National Aeronautics and Space Administration, Lewis Research Center for financially supporting this work.

Finally, I wish to dedicate this thesis to my wife, Patricia, without whose constant encouragement, patience and understanding this goal might not have been reached.

TABLE OF CONTENTS

LIST OF FIGURES

LIST OF TABLES

1.0 INTRODUCTION

Vertical take-off and landing (VTOL) aircraft are currently under study as a means for improving short-haul intercity air transportation systems. VTOL aircraft can relieve airport congestion, reduce air time delays, and can also supply access to communities currently without air transportation. The feasibility of VTOL intercity air transportation systems has been explored by a number of domestic and foreign organizations and government agencies[1,4*]. It is recognized that there are many aspects to the problem of VTOL transportation system - economic, sociological, and political, as well as technological[5].

The bulk of the research on VTOL transportation systems has been conducted on the technological problems. Some of the earliest wind tunnel test of lift fan concepts were performed in 1957 by Hickey for the National Advisory Committee for Aeronautics of the United States[6,7], Wardlaw, Templin and McEachern for the National Aeronautical Establishment of the National Research Council of Canada[8,9], and Gregory and Raymer for the National Physical Laboratory for the Ministry of Aviation, London, England[10]. These tests were performed on fans and propellers having low pressure ratios. They found that the lift and drag forces and pitching moment on the model could not be predicted by considering only the force reactions due to the fan momentum thrust and the wing lift. It was surmised

*Numbers refer to the references listed at the end of the report.

that part of these discrepancies could be accounted for by considering the changes in the flow field about the wing due to fan-wing interaction.

All three countries have continued research to determine the fan-wing-flow interactions. In England, the investigations were carried on with scale models having low fan-to-wing area ratios. Results of this work have been published in references 11 through 13. In Canada, tests were also performed on scale models[14]. In the United States the bulk of the work was carried out at Ames Research Center with large scale models[15,16]. Hickey (in reference 16) has proposed a rudimentary method for estimating the lift, drag and pitching moment which gives good agreement with his experimental work. Other NASA work on fan-in-wing concepts was performed by Mort[17] and Spreeman[18].

Norland[19] attempted to develop a two-dimensional theory to explain the decrease in lift at low forward speeds which has been indicated in small scale tests of fan-in-wing configurations. Correlation of Norland's theory with his experimental work is inconclusive, however it provided a basis for a sound theoretical treatment of the fan-in-wing problem.

Feasibility studies of V/STOL concepts for short-haul transports[1] has shown the need for advanced-concept lift fans that are quiet, smokeless, and reliable. To develop these advanced-concept lift fans requires detailed design data on the performance of advanced-concept lift fans in the transition speed range (crossflow

velocity) from vertical to normal wing-supported flight, There are a number of research problems associated with the performance of lift fans operating in the transition speed range. One problem, crossflow inlet distortion encountered during transition, has an adverse affect on lift-fan performance and noise generation. A second problem is the effect of crossflow velocity changing the back pressure at the exit of the lift fan which changes the operating point of the lift fan. A third problem is the interference effect of the interaction of the fan flow and external airflow.

NASA Lewis Research Center recently embarked on a research program to generate detailed design and performance data on advanced lift-fan concepts. An initial experimental test project measured the detailed crossflow performance of a 15-in. diameter lift-fan simulator installed in a two-dimensional wing. The fan-in-wing model tests were conducted in a 9- by 15-ft V/STOL wind tunnel[20].

Results of the measured fan axial force data and overall aerodynamic characteristics of the fan-in-wing configuration have been reported by Yuska and Diedrich[21]. The applicability of these results to the thesis topic will be discussed in other sections of the thesis.

Presently a report is in preparation to present the internal flow characteristic of the lift-fan simulator, and analysis is being conducted to determine the relationship between the axial force measured on the load cell force balance and the calculated

momentum thrust of the fan and turbine. In addition, tests have been completed on three other lift-fan simulator designs.

Since lift-fan simulator models are very expensive and test time is limited and expensive, it is desirable to develop a mathematical prediction model for the lift-fan simulator performance characteristics over its entire operating range.

The purpose of this thesis is to present the results of a multiple linear regression analysis prediction model for a 15-in. lift-fan simulator. The prediction model is developed from observed values of lift-fan simulator thrust loading and axial-force loading as the dependent variable and major test variables (cross-flow velocity, fan corrected tip speed and wing angle of attack) as the independent variables.

There are a number of ways that the prediction model may be used. A reliable prediction model could be used to reduce the number of test runs required to define the performance characteristics of the lift-fan simulator. The use of the prediction model would allow the experimental investigator to make better use of the available test time and reduce the cost of experimental test programs. The use of replicated data could provide an estimate of the accuracy to the test data. The prediction model could also be used in the design of future experimental lift fan simulators.

The prediction model would also be useful in smoothing the data for the analytical work of determining the relationship between the axial force measured on the load cell balance and the calculated

momentum thrust of the fan and turbine. This relationship is useful in the analysis to determine the interference effect of the fan flow and external airflow on the lift-fan simulator.

2.0 DESCRIPTION OF EXPERIMENT

The objective of the experiment was to determine the performance of a model VTOL lift-fan simulator installed in a two-dimensional wing section for various test conditions. The lift-fan simulator consists of a 15-in. diameter fan driven by a turbine contained in the fan hub. The wing section was designed to simulate the aerodynamic flow which would be produced by a VTOL transport aircraft during landing or take-off.

The performance of the lift-fan simulator is measured by the total axial thrust developed under various conditions. The total axial force, F, is the sum of the fan momentum thrust, F_F, lb; the turbine momentum thrust, F_T, lb; and the fan base force, F_B, lb or

$$F = F_F + F_T + F_B \tag{1}$$

The fan and turbine momentum thrust is calculated from observed values of total pressure, P, total temperature, T, and airflow angle, β, at the fan and turbine exit; and from observed values of static pressure, p_1, at the fan inlet which is correlated with fan weight flow, w_1, using a correlation equation from a theoretical technique developed by Stockman[22]; and from observed values of turbine weight flow, w_T, measured with an orifice plate. Another measure of fan performance was the axial force F_{LC} measured on a load cell force balance. The force balance consists of three 500 lb load cells equally spaced on a 22.5-in. diameter circle.

The load cell force balance attaches the lift fan simulator to the wing.

The major test variables were:

(1) Free-stream (airflow) velocity, V, feet per second (this parameter is also commonly called crossflow velocity in VTOL applications and may be used interchangeably).

(2) Fan corrected tip speed, $U_T/\sqrt{\theta}$ expressed as a percentage of the corrected tip speed at design conditions ($U_T/\sqrt{\theta}$ = 980 ft/sec). (Tip speed is the product of the angular velocity of the fan rotor blade times the tip radius of the rotor blade; and θ is the ratio of inlet total temperature to standard sea-level temperature of 518.7° R).

(3) Wing angle of attack, α, deg.

Tests were conducted at many possible combinations of test variables. However, the test conditions can be grouped into two major groups: (1) Static test conditions where the crossflow velocity is zero, and (2) crossflow test conditions where the crossflow velocity varied from 70 to 240 feet per second. For static test conditions, test data were observed at eight values of fan corrected tip speed and two angles of attack. For crossflow test conditions, test data were observed at six crossflow velocities, two values of fan corrected tip speed, and eleven values of angle of attack. Test data were observed at 52 points corresponding to different combinations of test points. Table I is a summary of the observed test conditions.

TABLE I

SUMMARY OF TEST CONDITIONS AND INPUT DATA

Crossflow velocity, V, ft/sec	Corrected tip speed, $U_T/\sqrt{\theta}$, percent of design speed	Angle of attack, α, deg	Total thrust loading, $F/\delta A$, lb/ft^2	Axial-force loading, $F/\delta A$, lb/ft^2	Force loading difference, $\Delta F/\delta A$, lb/ft^2
82.1	100.38	-10.10	758.2	701.7	-56.55
117.5	99.91	-10.11	731.4	691.2	-40.15
151.0	99.20	-10.11	709.9	660.3	-49.52
180.0	99.88	-10.29	702.6	667.0	-19.90
207.4	99.87	-10.12	692.0	672.0	-35.58
239.9	99.61	-10.16	690.4	677.1	-13.30
76.8	100.18	-0.22	760.9	716.3	-44.55
120.1	99.74	-0.20	731.0	709.8	-21.17
151.9	99.47	-0.17	711.3	682.4	-28.92
180.2	99.34	-0.24	698.9	687.9	-11.03
203.3	99.90	-0.15	700.1	722.0	21.95
236.4	99.21	-0.20	679.2	726.8	47.57
71.8	100.06	10.06	764.0	721.1	-42.85
118.3	99.57	10.06	739.5	725.6	-13.93
153.0	99.53	10.03	715.3	728.2	12.95
177.8	99.54	10.04	699.2	734.6	35.44
204.1	99.90	10.03	680.6	747.1	66.49
234.4	100.66	10.10	649.9	756.6	106.73
81.3	70.34	-10.10	376.6	343.7	-32.86
118.0	69.78	-10.10	375.8	333.6	-42.23
158.6	70.01	-10.20	378.8	342.6	-36.20
181.8	69.74	-10.20	380.3	357.4	-22.92
205.1	69.69	-10.10	377.8	370.3	-7.53
238.7	68.88	-10.20	382.0	391.2	9.21
78.0	70.27	-0.20	380.3	346.2	-34.07
121.8	70.25	-0.20	378.7	357.6	-21.08

TABLE I (Concluded)

SUMMARY OF TEST CONDITIONS AND INPUT DATA

Crossflow velocity, V, ft/sec	Corrected tip speed, $U_T/\sqrt{\theta}$, percent of design speed	Angle of attack, α, deg	Total thrust loading, $F/\delta A$, lb/ft^2	Axial-force loading, $F/\delta A$, lb/ft^2	Force loading difference, $\Delta F/\delta A$, lb/ft^2
151.3	69.78	-0.30	381.3	372.8	-8.50
178.5	69.85	-0.10	379.1	387.3	8.19
206.4	69.40	-0.20	385.5	412.3	26.78
237.2	69.23	-0.10	375.0	417.3	42.35
74.0	70.41	10.10	381.3	365.0	-16.33
120.5	70.20	10.10	378.4	376.8	-1.55
153.3	70.06	10.20	380.1	395.6	15.46
182.1	69.61	10.20	381.2	417.0	35.82
204.5	69.82	10.20	371.5	437.6	66.14
234.3	69.70	10.10	345.0	451.9	106.86
205.6	69.46	-13.60	381.4	355.9	-25.53
204.4	69.39	-5.10	379.7	386.8	7.06
207.5	69.73	4.90	377.1	434.1	56.99
204.4	69.84	15.50	348.3	440.6	92.30
204.2	99.75	-15.30	692.1	643.9	-48.20
204.4	99.93	-5.10	694.5	686.0	-8.50
201.5	100.23	5.00	691.5	726.9	35.40
204.6	99.15	15.50	667.8	766.0	98.20
0	70.83	0	411.4	347.9	-63.50
0	81.14	0	538.7	479.8	-58.90
0	85.89	0	613.3	542.4	-70.90
0	91.57	0	696.0	624.7	-71.30
0	96.28	0	762.6	691.7	-70.90
0	101.39	0	819.2	745.8	-73.40
0	106.18	0	860.1	802.3	-57.80
0	111.73	0	910.1	852.9	-57.20

3.0 EXPERIMENTAL MODEL AND APPARATUS

In this chapter, a detailed description of the experimental model and apparatus used in this experiment is presented. The test procedure, instrumentation, and data recording equipment used for data collection are described.

3.1 Wing and Wing Balance

A photograph of the fan-in-wing model installed in the 9- by 15-ft V/STOL test section is shown in Figure 1. The wing spanned the 9-ft height of the test section and had a 4.5-ft chord. The wing has a constant NACA 65_3A(218)-217 airfoil section along the span except for localized modifications required for fan installation.

The fan-in-wing model was attached to a wing balance that measures overall model lift, drag, and pitching moment. Figure 2 is a sketch of the wing balance showing pertinent dimensions.

3.2 Fan and Drive Turbine Characteristics

The fan assembly was attached to a force balance system within the wing. The fan force balance consists of three 500-lb load cells equally spaced on a 22.5-in. diameter circle, as shown in Figure 3. The balance measured the combined axial force of the fan and turbine. Drive air was supplied from both sides of the wing.

Figure 4 shows a cross section of the model lift fan. The fan rotor tip diameter was 15.2 in., and the stage exit diameter was

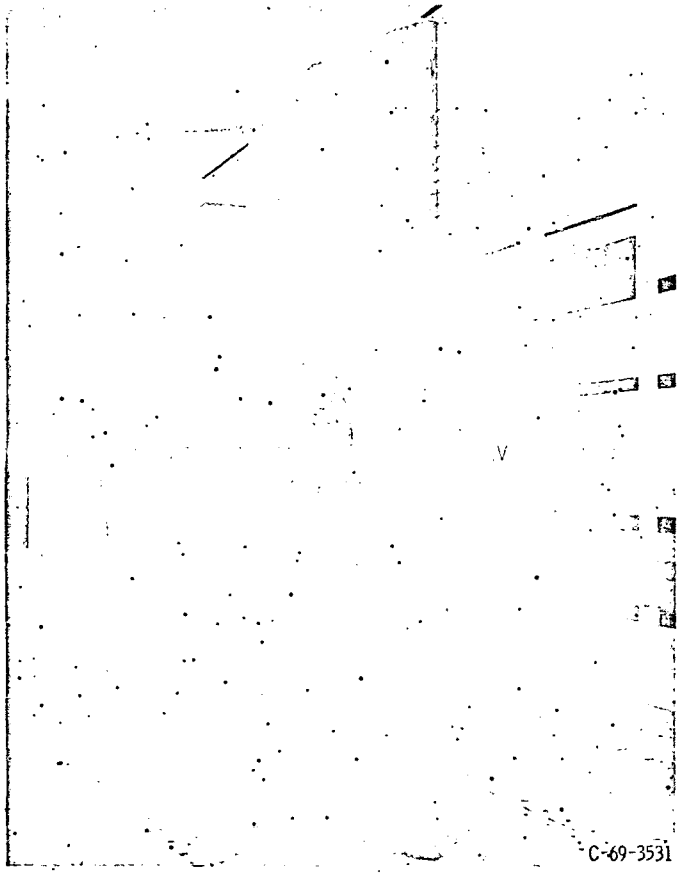

Figure 1. - Fan-in-wing model in 2.74- by 4.58-meter (9- by 15-ft) V/STOL wind tunnel.

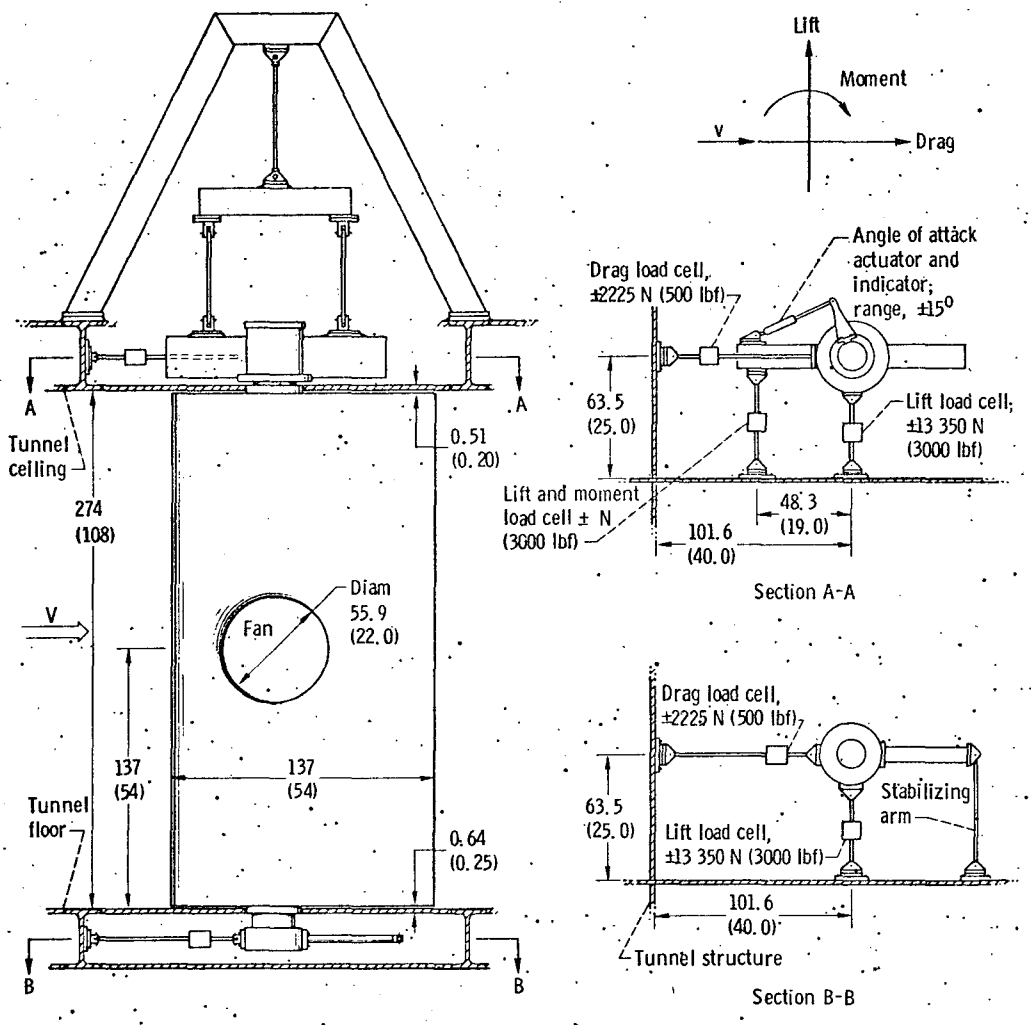

Figure 2. - Wing balance. (All dimensions are in cm (in.).)

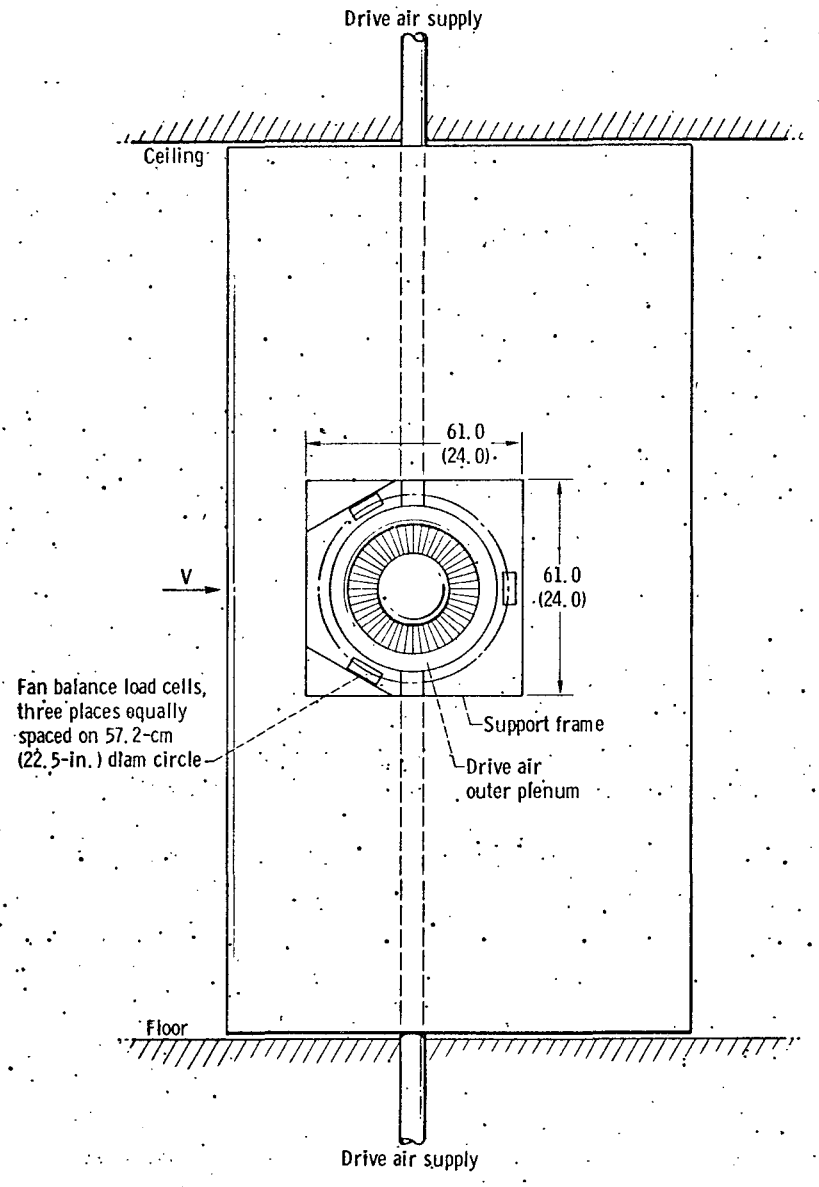

Figure 3. - Fan-in-wing installation on fan balance. (All dimensions are in cm (in.).)

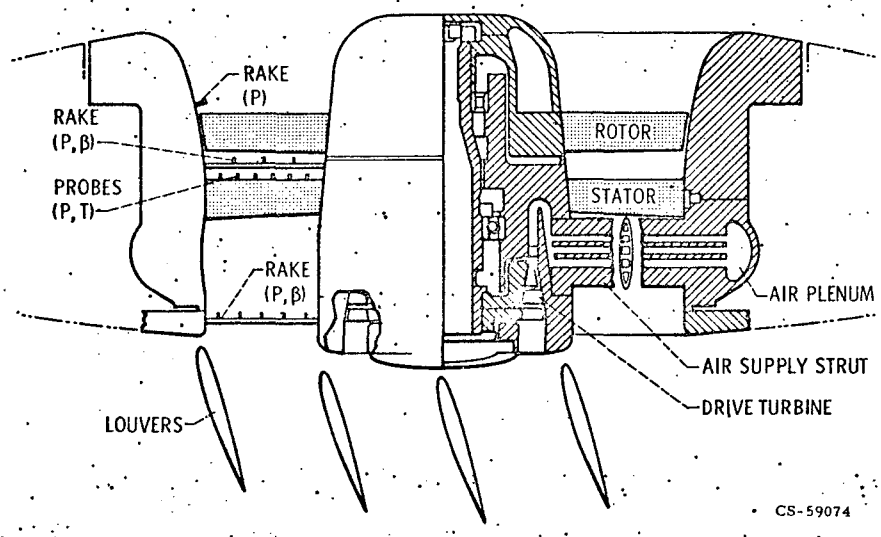

Figure 4. - Gross section of 15-inch model lift fan.

14.78 in. The diameter of the fan inlet bellmouth at the wing junction was 22.0 in. The fan inlet bellmouth was contoured flush with the wing upper surface. The fan hub protruded from the wing lower surface as shown in Figure 4. The inlet and exit flow area of the fan stage were 0.990 ft^2 and 0.868 ft^2, respectively. The fan rotor had 35 blades which were made from 18 Nickel-200 maraging steel. Two 0.060-in. diameter damper wires located at 60 percent of the passage height from the hub provided sufficient damping to prevent blade flutter and reduce blade vibration.

The fan drive was a compact, two-stage supersonic turbine contained in the fan hub. The turbine was scaled from a previous NASA design[23,24]. The turbine had a mean diameter of 5.4 in. and developed 685 hp to drive the fan at design conditions. The turbine was driven by high-pressure air supplied through six equally-spaced struts (12.5 percent thickness ratio) spanning the fan passage (Fig. 4). The struts connected the inner and outer 360° plenums.

For some tests, exit louvers were mounted on the wing as shown in Figure 5. For this installation, the louver forces appeared only on the wing balance and not on the fan balance. The exit louvers covered both the fan and drive turbine exhaust. The exit louvers were capable of remotely vectoring the fan and drive turbine thrust from 3° forward (negative louver angle of attack) to 40° aft (positive louver angle of attack).

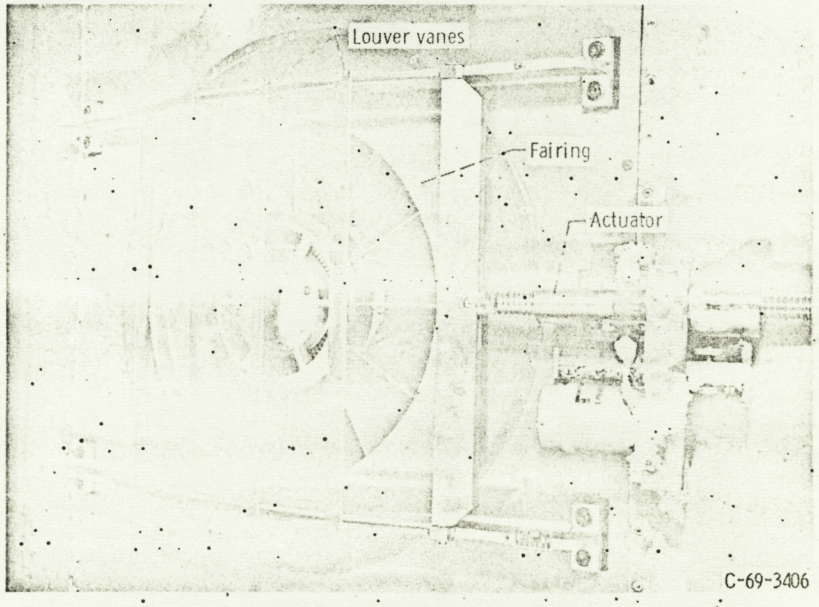

Figure 5. - Exit louver installation.

3.3 Instrumentation for Data Collection

The major features of fan internal instrumentation are shown in Figure 4. Static pressure taps were located at eight circumferential positions on the outer shroud of the fan inlet bellmouth 3/4 of an inch above the fan rotor leading edge. These eight static pressure measurements were averaged together to provide an average inlet static pressure for use in the weight flow correlation. At the rotor exit, six equally spaced stator blades were each instrumented with total temperature probes at three radial positions.

At the duct exit, six fixed-position rakes equally spaced around the circumference (positioned between the turbine drive-air struts) were used to measure the airflow angle at three radial positions and total pressure at five radial positions as shown in Figure 6. Static pressure taps were located at six equally-spaced positions on the hub and tip surfaces in the measuring plane of the total pressure probes. The airflow angle probes were fixed-position, non-nulling instruments. The construction details and calibration techniques for fixed-position flow direction probes are reported in reference 25.

The turbine exit duct was instrumented at two circumferential locations to measure flow angle at one radial position, total pressure at five radial positions, and total temperature at two radial positions (Fig. 7). Two equally-spaced static taps were located on the turbine exit inner and outer wall surfaces. Turbine air weight flow was measured by a calibrated flat plate orifice. Base static

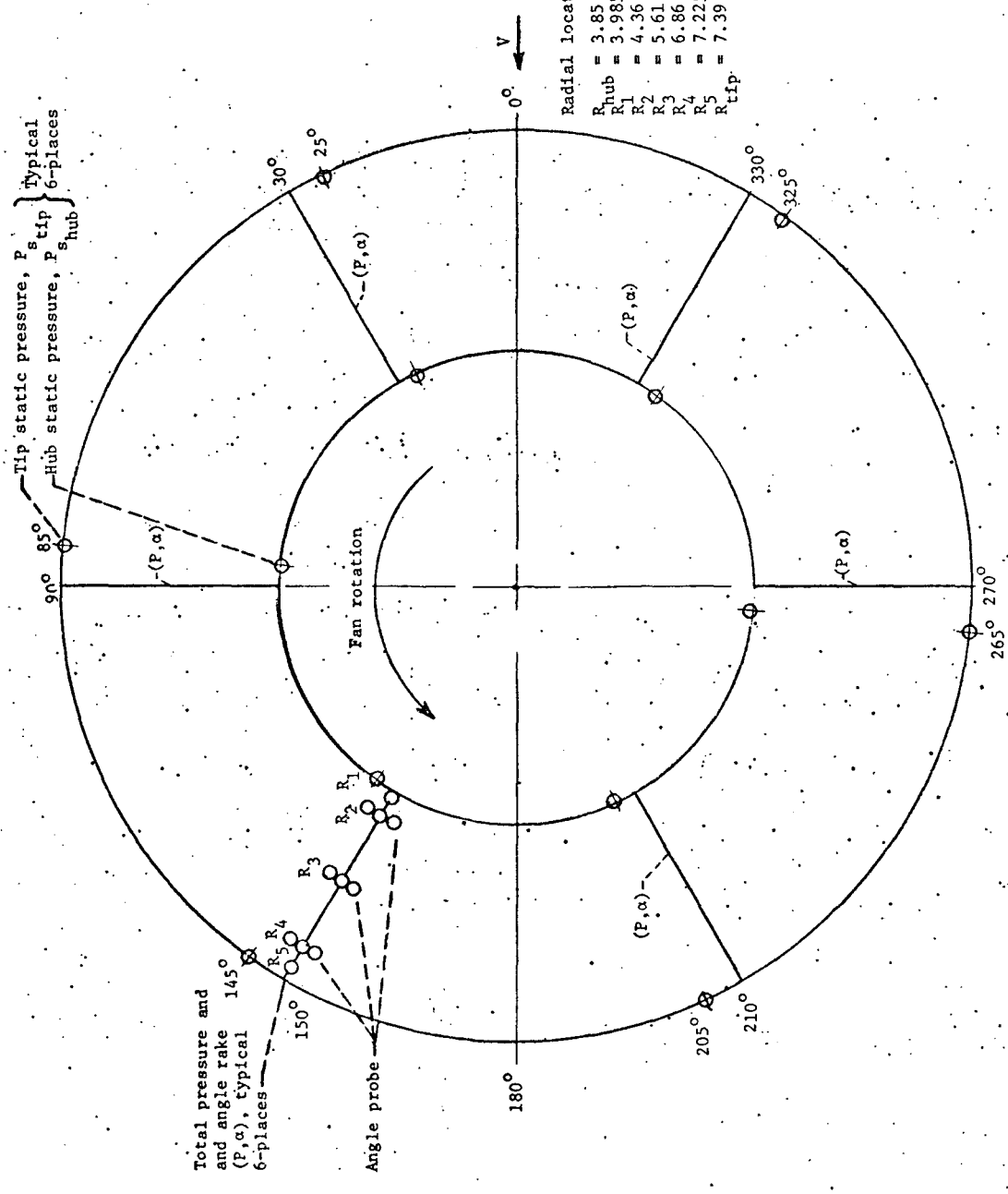

Figure 6. - Fan Duct Exit Plane Instrumentation Location.

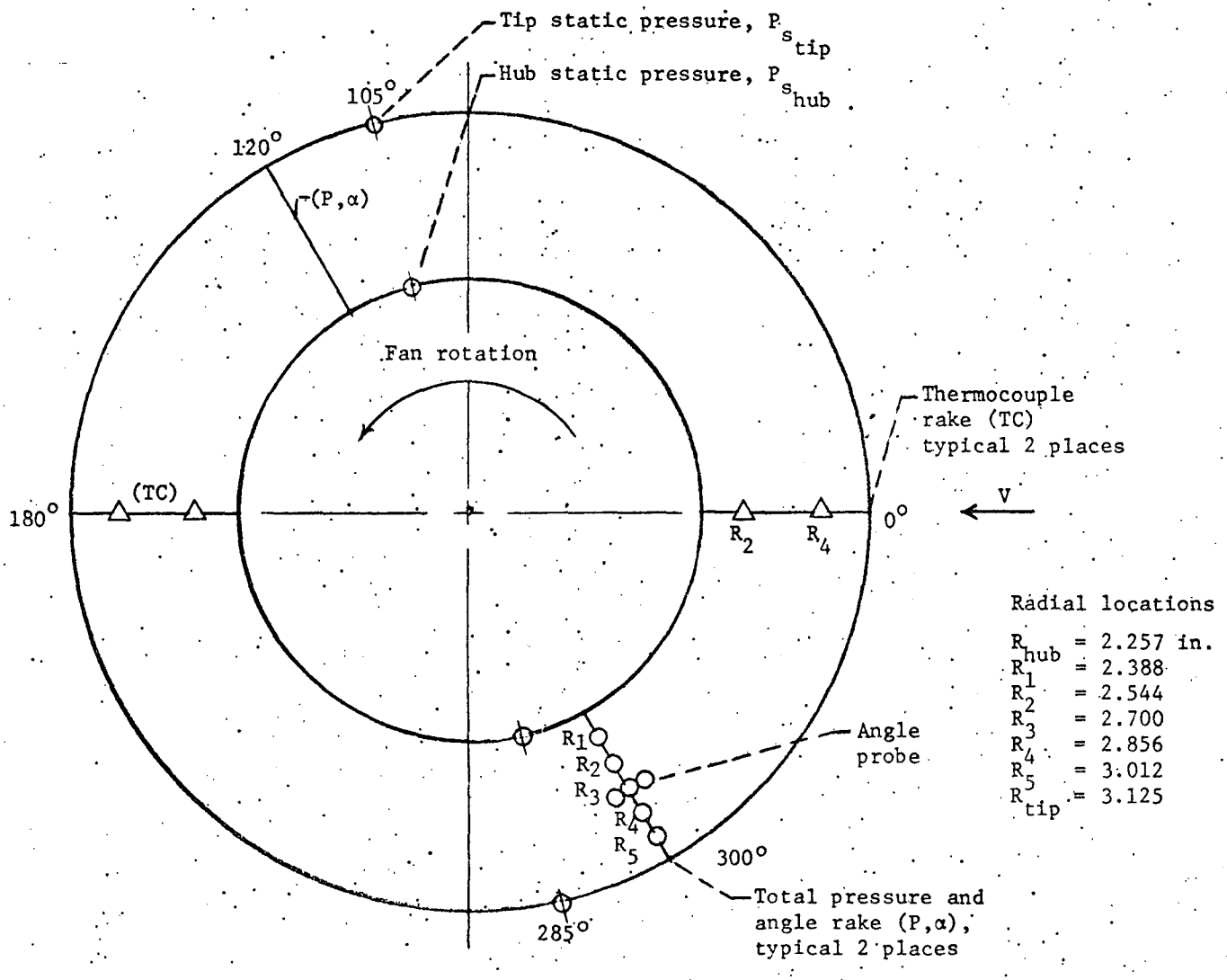

Figure 7. – Turbine Exit Plane Instrumentation Location.

pressures were measured on the ring between the fan and turbine flow passages and on the centerbody surface of the turbine. These static pressures were used to calculate the fan base force.

A summary of the total instrumentation provided for in the experiment is shown in Table II and Table III. A total of 313 pressures and 31 temperatures were measured. To reduce the number of strain gage pressure transducers required to measure the 313 pressures, a scanning type pressure sampling valve for measuring multiple pressures was used.

Each valve is recorded in sequence and controlled by the data recording system. The valve rotor is then stepped to the next port for the next measurement. The process is repeated until all pressures are measured. The stepping rate may be varied to match the settling out time for the pneumatic pressure system. The transducer signal is connected to the automatic voltage digitizer and to the data recording system. With this system one pressure transducer can measure 46 individual pressures. In this experiment seven pressure sampling values were used. Each using only one pressure transducer. Thirty two additional transducers were used to measure various required gage and absolute pressures, and pressures beyond the measurement range of the transducers in the sampling valves. Thus, only 39 pressure transducers were used to measure 313 pressures.

TABLE II

SUMMARY OF TOTAL NUMBER AND TYPE OF PRESSURE AND TEMPERATURE MEASUREMENTS

Location of instrumentation in lift-fan simulator	Total number of pressure measurements				Total number of temperature measurements	
	P_s	P	ΔP	P_A	T	ΔT
Wing surface	24				3	
Bellmouth front	40					
Bellmouth rear	24	12				
Rotor exit plane	12	54	18	18		18
Duct exit plane	12	30	18	18		
Turbine inlet orifice	1		3		1	
Turbine inlet header	1				3	
Turbine inlet plenum	1					
Turbine exit plane	4	10	2	2	4	
Fan exit lower surface	3					
Tunnel conditions	3		3		2	
TOTAL	125	106	44	38	13	18

TABLE III

SUMMARY OF TOTAL NUMBER AND TYPE OF FORCE AND MISCELLANEOUS DATA MEASUREMENTS

Type of measurement	Total number of measurements
Lift force	3
Drag force	2
Axial force	3
Fan RPM	1
Fan torque	1
Wing angle of attack	1
Louver position	1
Fan box static pressure	1
Rotor strain	2

3.4 Data Recording Equipment

The data is recorded on the Lewis Research Center central data recording system called the Central Automatic Digital Data Encoder (CADDE) that is used by many test facilities to record digital readings from transducers of pressure, voltage, and events per unit time. A schematic of the system is shown in Figure 8, and reference 26 gives a detailed description of the system. The system has a 500-data word capacity. In this experiment 368-data words were recorded at each test point. The data are recorded on magnetic tape as binary-coded decimal digits with additional characters for identification and computation instructions. The magnetic tape is the permanent record of the raw data. In addition, the data may be simultaneously recorded on an IBM 360 time-sharing computer system. This allows the test engineer to receive "on-line" computer data typed out in the control room after the data point is taken. After recording, a duplicate tape is made to process the data as a stored program on an IBM 7094 computer.

3.5 Experimental Test Procedure

The general test procedure was to set the desired test conditions of crossflow velocity, corrected tip speed, wing angle of attack, and exit louver deflection angle. The fan internal flow and tunnel flow conditions were allowed to stabilize at a steady state condition before the start of each data recording point. The time to acquire data (data scan time) for a single test point was typically about 25 seconds. During the data acquisition period,

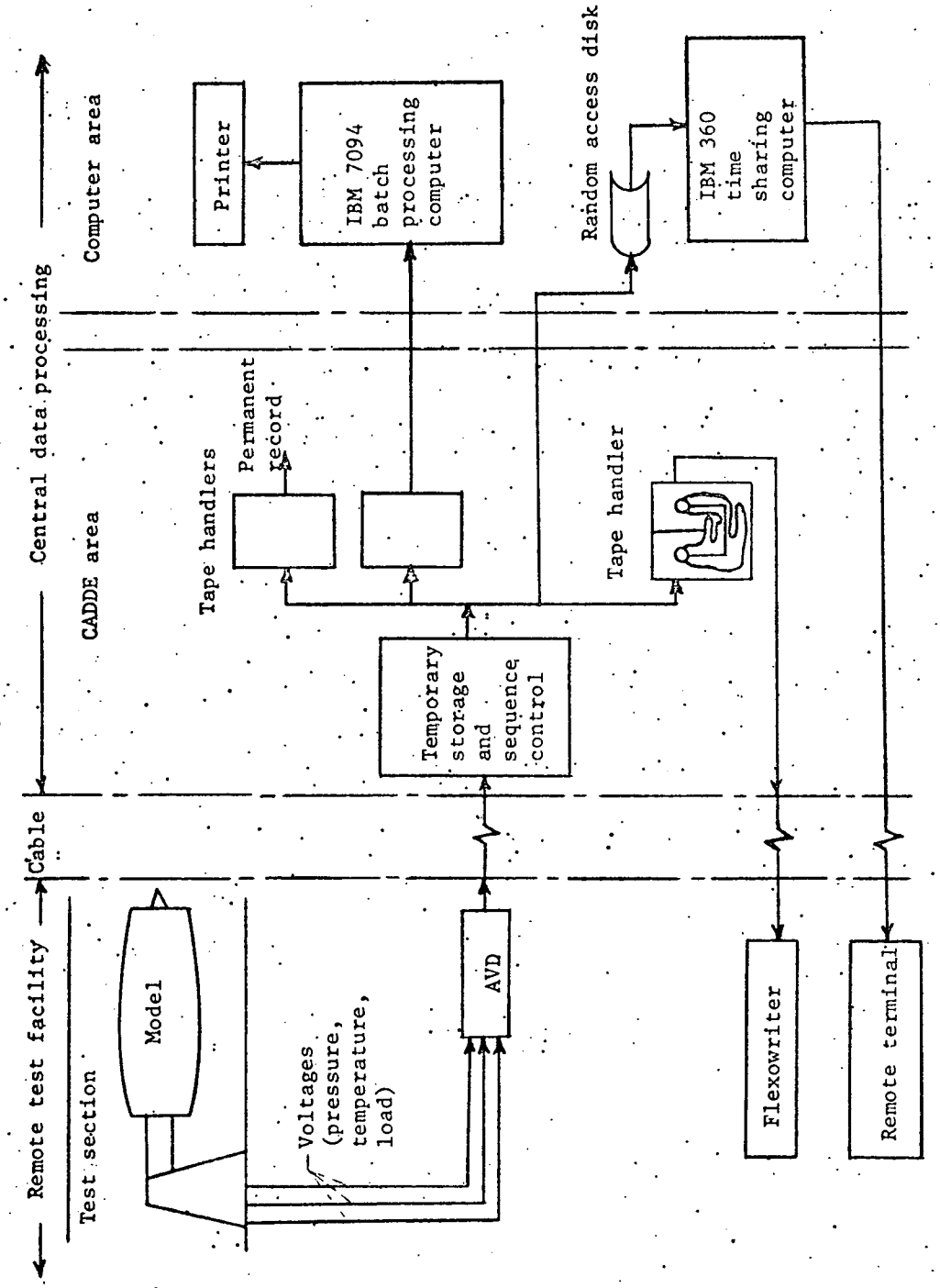

Figure 8. - Schematic Diagram of Data Processing System.

test conditions were stabilized through the individual control systems for each of the preceding independent parameters. The fan speed generally fluctuated somewhat during the data acquisition time. Over the speed range, the variation was ± 50 rpm which was only a ± 0.3 percent variation of the design speed.

Test Procedure for Static Test Conditions (Zero Crossflow Velocity)

The tunnel circuit was vented to the atmosphere to minimize recirculation of the fan exhaust. Static tests were conducted with the fan axis both perpendicular and parallel to the tunnel axis. The orientation with the fan axis parallel to the tunnel axis and the inlet of the fan facing upstream was used to achieve the most steady flow conditions at the fan inlet. Data taken with the fan axis perpendicular to the tunnel axis showed that the internal flow of the fan was less steady than with the fan axis oriented parallel to the tunnel axis, although the overall thrust levels were the same for both orientations.

Test Procedure for Crossflow Test Conditions

The general test procedure was to first bring the tunnel up to speed and set the desired level of crossflow velocity in the test section. Before the start of each data recording point, the tunnel flow was allowed to stabilize for several minutes while the desired values of wing angle of attack, louver position, and fan speed were established.

4.0 DATA ANALYSIS TECHNIQUES

This chapter describes the data analysis procedure used in developing a prediction model for the lift-fan simulator. The dependent variables, total axial force, F, and the axial force measured on the load cell force balance, F_{LC}, were calculated for the various test variables. The details of these calculations are presented in Appendix A. To enable the test results of various lift fans to be compared, the total axial force and the axial force measured on the load cell balance are divided by the fan frontal area, A = 1.263 ft^2, and δ the ratio of inlet total pressure to standard sea-level pressure of 2116.2 lb/ft^2. The resulting ratio, $F/\delta A$ or $F_{LC}/\delta A$ is the total thrust loading parameter or the axial-force loading parameter, respectively. These parameters normalize the data so that the results from this lift-fan simulator test can be compared to the test results of other lift-fan simulators or full-scale lift fans having different fan frontal areas.

The calculated dependent variables and the independent test variables were then used as input data (shown in Table I) to determine the lift-fan simulator prediction model. A multiple linear regression computer program (RAPIER)[27], which is a program in the NASA Lewis Research Center computer program library, was used to compute the lift-fan simulator prediction model equation. A description of the multiple linear regression computer program is presented in Appendix B.

The model equation was assumed to be

$$y = b_0 + b_1 V + b_2(U_T/\sqrt{\theta}) + b_3\alpha + b_4 V(U_T/\sqrt{\theta}) + b_5 V\alpha + b_6(U_T/\sqrt{\theta})\alpha + b_7 V(U_T/\sqrt{\theta})\alpha + b_8 V^2 + b_9 V^2\alpha + e \quad (2)$$

where y is the dependent variable corresponding to $F/\delta A$ or $F_{LC}/\delta A$; b_0, b_1, $\cdots b_9$ are the regression coefficients and e is the error term. The computer program was then used with the backward rejection option to delete regression coefficients that have t-statistics which are less than 90 percent significant. The program then computes the final regression coefficients, the analysis of varience (ANOVA) table and the coefficient of correlation, r. An F test is made for testing the null hypothesis H_0: that there is no correlation, that all the correlation coefficients are zero. The alternative hypothesis is H_1: that there is a significant correlation. If the calculated value of F is greater than the critical value of the F distributions for the number of degrees of freedom and the specified significance levels, then the null hypothesis H_0 is invalid indicating that there is a significant correlation and the regression coefficients are not zero. The program then computes a calculated response (y) for each set of independent variable observations using the prediction model equation. A comparison is then made between the observed values and the calculated values.

Since there was an observed difference between the total axial force loading and the axial-force loading measured on the load cell balance, another dependent variable was calculated for all test variables (see Table I). This variable is called the force loading difference, $\Delta F/\delta A$, which is the difference between $F_{LC}/\delta A$ and $F/\delta A$.

$$\Delta F/\delta A = F_{LC}/\delta A - F/\delta A \qquad (3)$$

The multiple linear regression computer program was again utilized to determine if a correlation existed for force loading difference as a function of the independent test variables.

The RAPIER computer program also has a prediction option, which used the regression equation to predict an estimated response at some condition of the independent variables. This option is useful in calculating responses at fixed values of the independent variables. This technique is useful in making carpet plots to allow the presentation of the dependent variable as a function of all its independent variables on a single graph.

5.0 RESULTS AND DISCUSSION

In this chapter, the results of the multiple linear regression analysis are presented. The correlations were obtained for total thrust loading, axial-force loading, and the difference between the axial-force loading and total thrust loading. In each of the above cases the independent variables were crossflow velocity, corrected tip speed, and angle of attack. In addition a final correlation was obtained for the total thrust loading as a function of axial-force loading. The results of the statistical computations are discussed, and a comparison of the correlation equations and the observed values is presented. The physical significance of the observed variations in loading parameters are also interpreted for the model VTOL lift-fan simulator.

5.1 Correlation Equations

The prediction model correlation equation for each dependent variable was computed using the input data shown in Table I. The resulting correlation equations are shown in Table IV. From Table IV it can be seen that in each correlation equation for total thrust loading, axial-force loading, and force loading difference, certain regression coefficients were deleted by the backward rejection option of the computer program because the t-statistics test of each delected regression coefficient showed a significance level of less than 90 percent.

TABLE IV

CORRELATION EQUATIONS

1. Total thrust loading:

$$F/\delta A = -529.2807 + .8361\ V + 13.1970\ (U_T/\sqrt{\theta}) - .0132\ V(U_T/\sqrt{\theta}) + .01586\ V\alpha - .00010\ V^2\alpha \quad (4)$$

2. Axial-force loading:

$$F_{LC}/\delta A = -566.0920 + .9242\ V + 12.9196\ (U_T/\sqrt{\theta}) - .0132\ V(U_T/\sqrt{\theta}) + .02823\ V\alpha - .02678\ (U_T/\sqrt{\theta})\alpha + .000268\ V(U_T/\sqrt{\theta})\alpha + .00158\ V^2 - .00011\ V^2\alpha \quad (5)$$

3. Force loading difference:

$$\Delta F/\delta A = -38.7907 + .1294\ V - .2679\ (U_T/\sqrt{\theta}) + .000079\ V(U_T/\sqrt{\theta})\alpha + .00141\ V^2 + .00007\ V^2\alpha \quad (6)$$

4. Total thrust loading as a function of axial-force loading:

$$F/\delta A = 2.697 + 1.016\ F_{LC}/\delta A \quad (7)$$

Equations 4 and 5 in Table IV show that velocity V and tip speed $U_T/\sqrt{\theta}$ are the dominant independent variables in the equations for total thrust loading and axial-force loading. In both equations the regression coefficients associated with V and $U_T/\sqrt{\theta}$ are positive and have nearly the same value. The equations for total thrust loading (equation 4) also contains three interaction terms ($V(U_T/\sqrt{\theta})$, $V\alpha$ and $V^2\alpha$). The equation for axial-force loading (equation 5) contains six interaction terms ($V(U_T/\sqrt{\theta})$, $V\alpha$, $(U_T/\sqrt{\theta})\alpha$, $V(U_T/\sqrt{\theta})\alpha$, V^2, and $V^2\alpha$). These interaction terms account for the observed variations (increases and decreases) in total force loading and axial-force loading which will be discussed in a later section of this report.

Equation 6 in Table IV shows that velocity V and tip speed are again the dominant independent variables in the force loading difference equation. The equation also contains three interaction terms ($V(U_T/\sqrt{\theta})$, V^2, and $V^2\alpha$). The regression coefficients of the interaction terms are all positive which indicates that at a constant tip speed as V and α increase the value of $\Delta F/\delta A$ will increase. The observed increase in $\Delta F/\delta A$ with increasing V and α will be discussed later. The correlation equation for total force loading as a linear function of axial-force loading is shown in equation 7 of Table IV.

For each regression equation, the correlation coefficient was calculated; and the null hypothesis H_0: that there is no correlation, was tested. An F-test was performed, where the calculated

F value is compared to the critical value of the F distribution obtained from Table 7.9 in reference 28 for a 0.01 probability of a larger value of F and the computed number of degrees of freedom. The critical value of F is denoted as $F_{0.01,\nu_2,\nu_1}$ where the subscript 0.01 is the specified probability level; and ν_2 is the degrees of freedom for the mean squares of the regression; and ν_1 is the degrees of freedom for the mean squares of the residual. The results of the Analysis of Variance are shown in Table V. In each correlation equation for total thrust loading, axial-force loading, and force loading difference, the F-test showed that for each of these three correlation equations, the computed value of F was greater than the critical value of the F-distributions for the specified probability level of 0.01. Therefore, the null hypothesis H_0: that there is no correlation, that all the coefficients are zero, was rejected; and the alternative hypotheses H_1: that there is a significant correlation, was accepted. In each case, the correlation coefficient was greater than 0.988 which again indicates that there is a significant correlation for each dependent variable.

The correlation equation for total force loading as a function of axial-force loading was assumed to be linear. This assumption would probably be valid for zero crossflow conditions but not for nonzero crossflow conditions. It has already been seen that the effect of crossflow velocity on both loading parameters is nonlinear. Previous experience has not shown how the total thrust loading varies as a function of axial-force loading. Even with the

TABLE V

RESULTS OF ANALYSIS OF VARIANCE

Dependent variable	Source	Sums of squares	Degrees of freedom	Mean squares	$F_{computed}$	F_{table}	Correlation coefficient	Comments
Total thrust loading, $F/\delta A$	Regression	1599578.17	5	319915.633	3082.1	3.44	0.9985	Significant correlation
	Residual	4774.70605	46	103.797957				
Axial-force loading, $F_{LC}/\delta A$	Regression	1437502.97	8	179687.871	2457.8	2.93	0.9989	Significant correlation
	Residual	3143.64771	43	73.1080856				
Force loading difference, $\Delta F/\delta A$	Regression	116950.000	5	23390.0000	393.5	3.40	0.9885	Significant correlation
	Residual	2733.66864	46	59.4275789				
Total force loading as a function of axial-force loading	Regression	1484926.41	1	1484926.41	620.9	7.17	0.9620	Significant correlation
	Residual	119577.671	50	2391.55338				

linear assumption, the correlation equation for total thrust loading as a function of axial-force loading has a high degree of correlation. The correlation coefficient r is 0.9620, and the overall F-test indicated that the alternative hypothesis H_1: that there is a significant correlation, should be accepted.

5.2 Comparison of Correlation Equations and Observed Values

The values calculated from the correlation equation and the observed values of the dependent variable for the various test variables are compared. The comparison of the calculated and observed values for the total thrust loading and the axial-force loading are shown in Figures 9 thru 12. The data on Figure 9 shows that at zero crossflow velocity and 100 percent of design speed, the calculated value of total thrust loading is 809 lb/ft^2 as compared to the observed value of 819 lb/ft^2. At 70 percent of design speed (Fig. 10) the calculated value of total thrust loading is 405 lb/ft^2 as compared to the observed value of 411 lb/ft^2. The data also shows that the calculated values show the same trends with increasing crossflow velocity as the observed values.

The data on Figures 11 and 12 show that at zero crossflow velocity the calculated and observed values of axial-force loading are almost identical. Over the crossflow range tested, there is good agreement between the calculated and observed values, except at zero angle of attack and 100 percent of design speed test conditions. At these test conditions, the observed values appear to

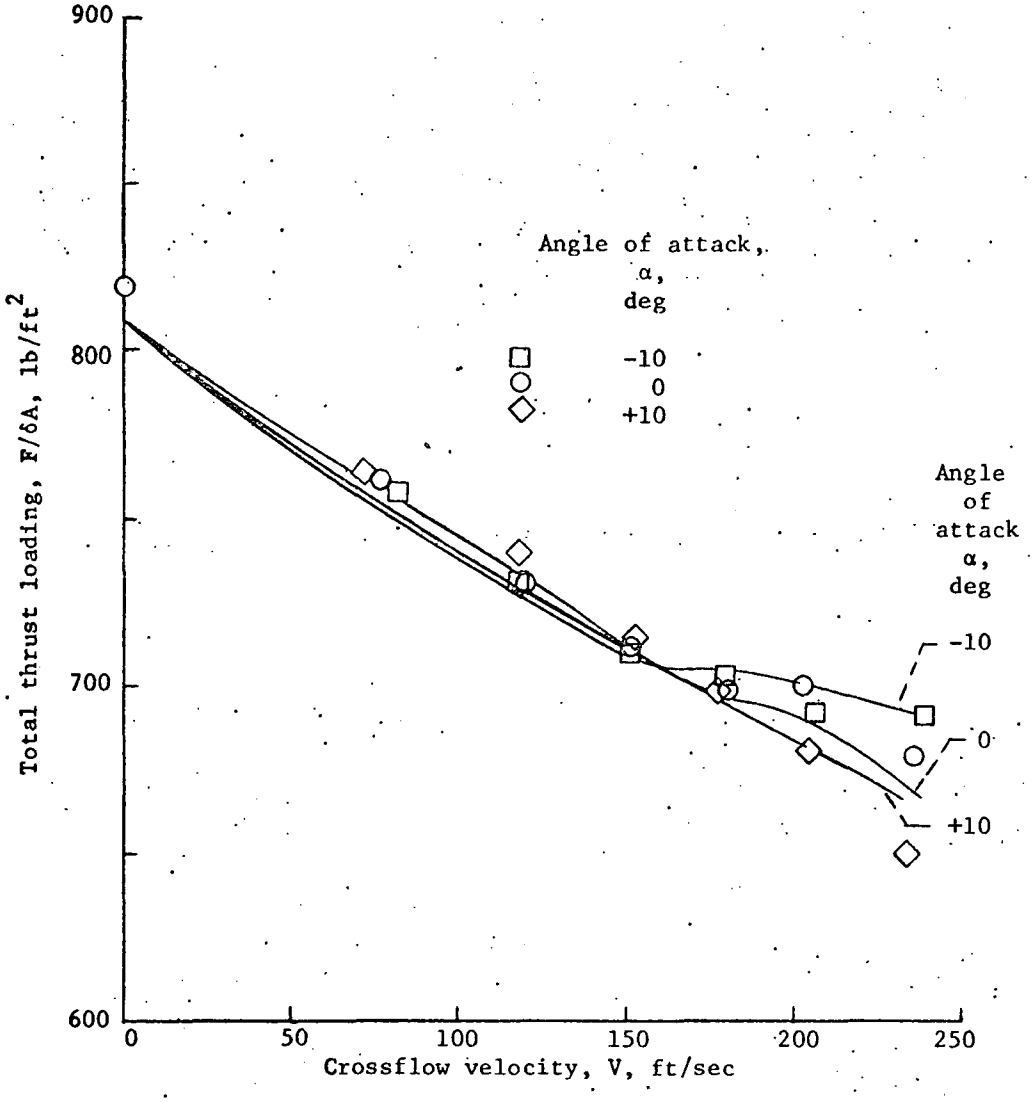

Figure 9. - Comparison of Computed Values from Correlation Equation and Observed Values of Total Thrust Loading at 100 Percent of Design Speed.

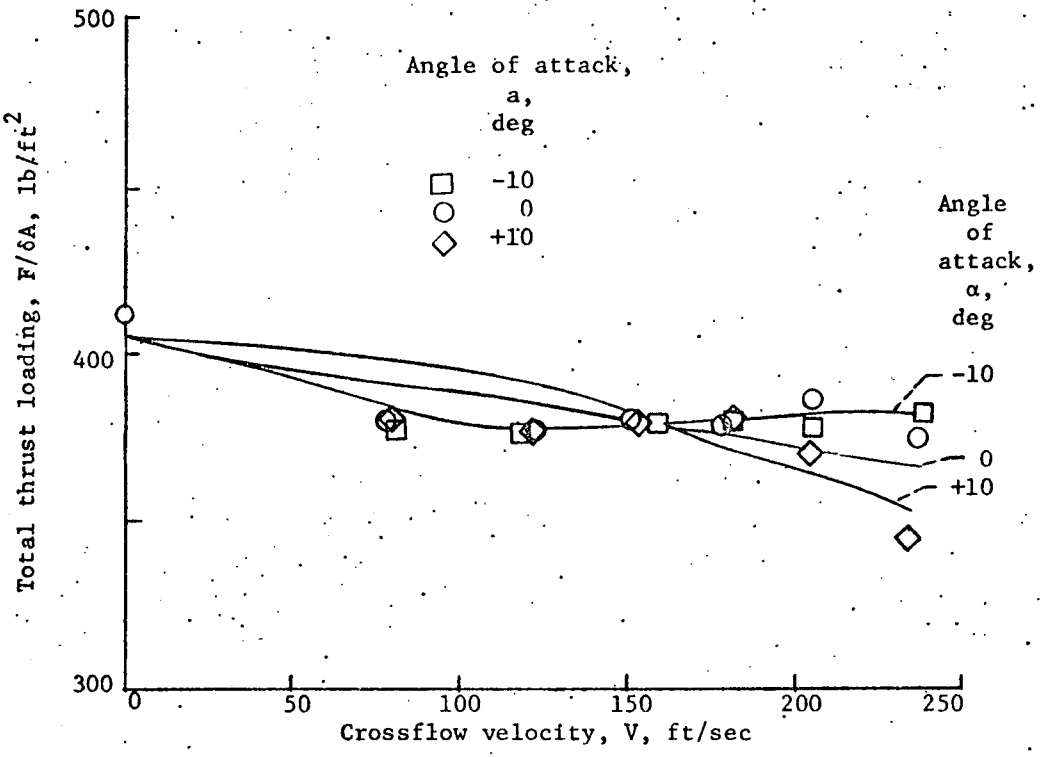

Figure 10. - Comparison of Computed Values from Correlation Equation and Observed Values of Total Thrust Loading at 70 Percent of Design Speed.

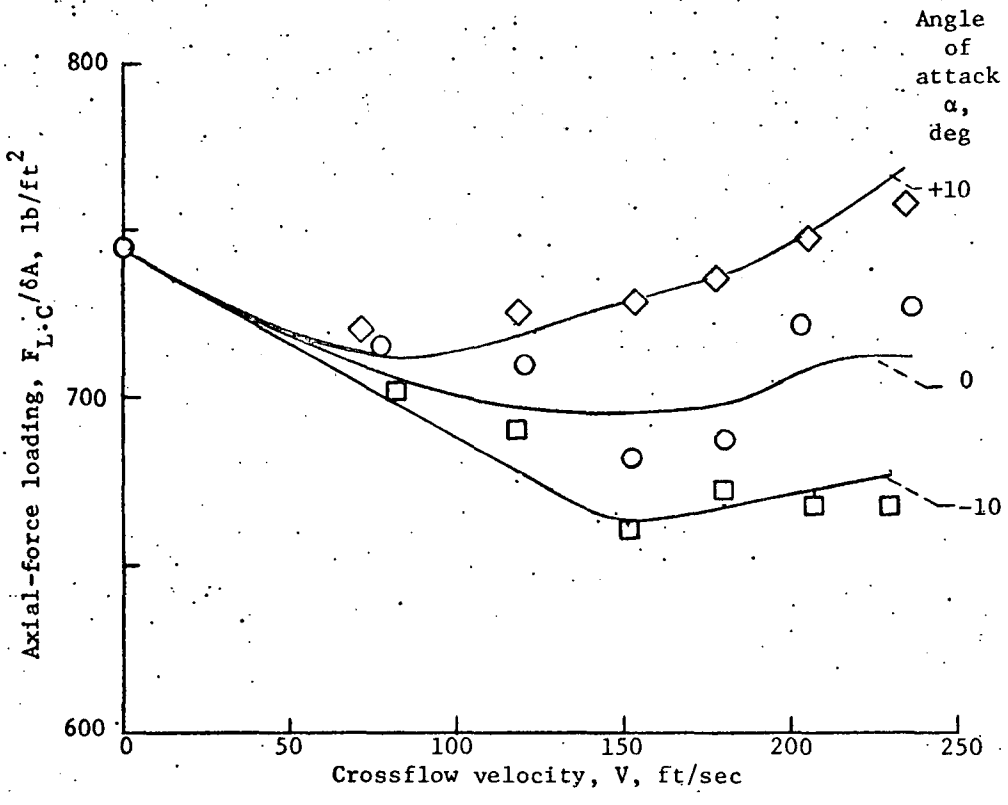

Figure 11. - Comparison of Computed Values from Correlation Equation and Observed Values of Axial-Force Loading at 100 Percent of Design Speed.

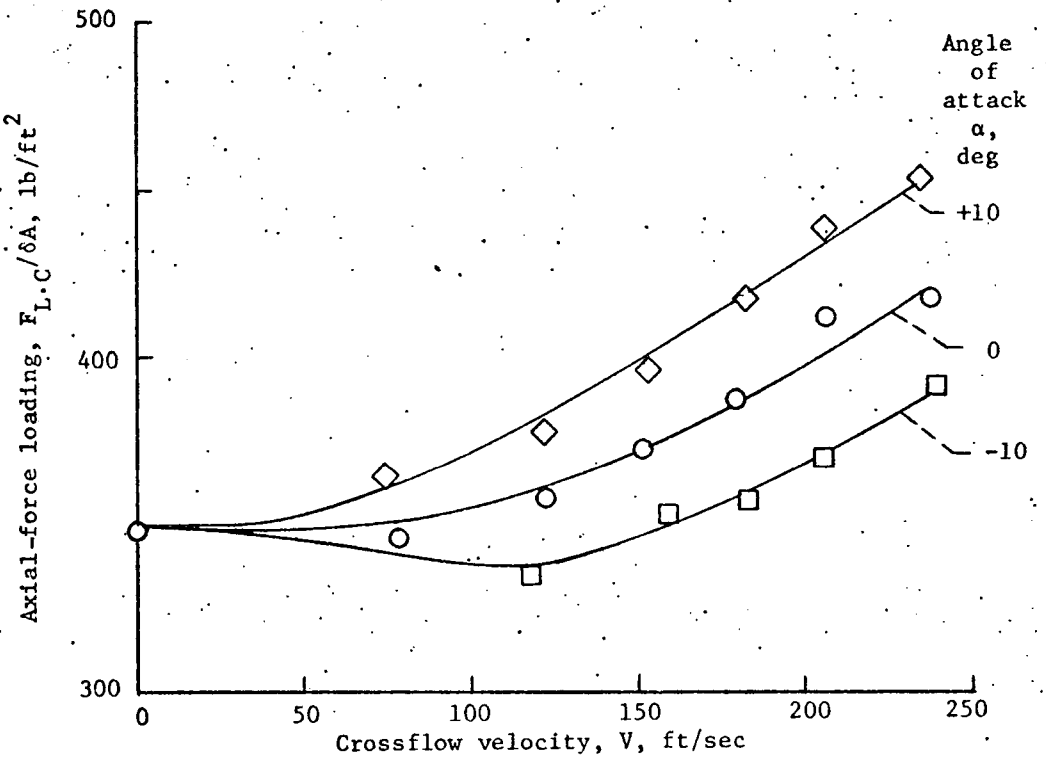

Figure 12. - Comparison of Computed Values from Correlation Equation and Observed Values of Axial-Force Loading at 70 Percent of Design Speed.

have more scatter than at the other test conditions. However, no reason could be found for this apparent deviation.

The values calculated from the correlation equation will now be used to discuss the variation in loading parameters with the various test variables. The data on Figures 9 and 11 show that at zero crossflow velocity for 100 percent of design speed, the total thrust loading is 809 lb/ft^2 as compared to the axial-force loading value of 744 lb/ft^2. At 70 percent of design speed (Figs. 10 and 12), the total thrust loading is 405 lb/ft^2 as compared to the axial-force loading of 350 lb/ft^2. This observed difference can be attributed to the fact that a portion of the fan momentum thrust acts on the wing because the inlet bellmouth of the lift-fan simulator is not of an infinite diameter. If the inlet had an infinite diameter, then the maximum lift force generated would be equal to the exit momentum thrust less the fan base force. Consequently, in this experiment, the full momentum thrust will not be measured on the load cell force balance resulting in a reduced value of axial-force loading.

A comparison of the data on Figures 9 thru 12 show that the effect of increasing crossflow velocity is not the same for total thrust loading as for axial force loading. At 100 percent of design speed and zero angle of attack (Fig. 9), the total thrust loading decreases uniformly from 809 lb/ft^2 at zero crossflow velocity to about 655 lb/ft^2 at the highest crossflow velocity of 240 ft/sec. However, the axial-force loading (Fig. 11) tends to decrease slightly (from 744 lb/ft^2 at zero crossflow

velocity) with increasing crossflow velocity to minimum value of 696 lb/ft^2 at about 150 ft/sec. Further increases in crossflow velocity to 240 ft/sec cause an increase in axial-force loading approaching the same level as that obtained at zero crossflow velocity.

At 70 percent of design speed (Fig. 10), the total thrust loading decreased slightly with increasing velocity. However, the axial-force loading (Fig. 12) increased uniformly with increasing crossflow velocity. For example, at zero angle of attack, the axial-force loading increased from 350 lb/ft^2 at zero crossflow velocity to a value of 420 lb/ft^2 at the highest crossflow velocity of 240 ft/sec.

The observed difference in trends between total thrust loading and axial-force loading with increasing crossflow velocity may be partially explained by the fact that crossflow velocity may effect the total thrust loading in two ways. First, crossflow velocity tends to cause flow separation in the fan inlet. Inlet flow separation was actually observed in this experiment. When flow separation occurs it reduces the effective flow area of the fan which reduces the weight flow through the fan. The inlet area blocked by flow separation increased with increasing crossflow velocity and increased angles of attack. Inlet flow separation was also found to be a function of corrected tip speed since more inlet flow separation was observed at the design tip speed (980 ft/sec) than at 70 percent of design tip speed.

The second effect of crossflow is to produce flow distortions at the inlet and within the fan flow passage. This effect reduces the overall total pressure at the exit of the fan. Both of these effects reduce the total thrust loading, and can explain the reason for the observed decrease in total thrust loading with increasing crossflow velocity and increasing angle of attack.

A comparison of the correlation equation and the observed values of the force loading difference is shown in Figures 13 and 14. The data show that at zero crossflow velocity the total thrust loading is greater than the axial force loading at both 100 and 70 percent of design speed. The correlation equation shows that at 100 percent of design speed (Fig. 13), the difference is -65 lb/ft^2; and at 70 percent of design speed (Fig. 14) the difference is -58 lb/ft^2. The reason for the difference has been explained by the previous discussion.

The data in Figures 13 and 14 show that the force loading difference increases uniformly with increasing crossflow velocity, and that the force loading difference increases more rapidly at $+10^{o}$ than at -10^{0} angle of attack.

A comparison of the correlation equation and observed data for total thrust loading as a function of axial-force loading is presented in Figure 15. The data showed that at zero crossflow velocity, the observed data is displaced by about a constant value from the correlation equation. The effect of angle of attack and

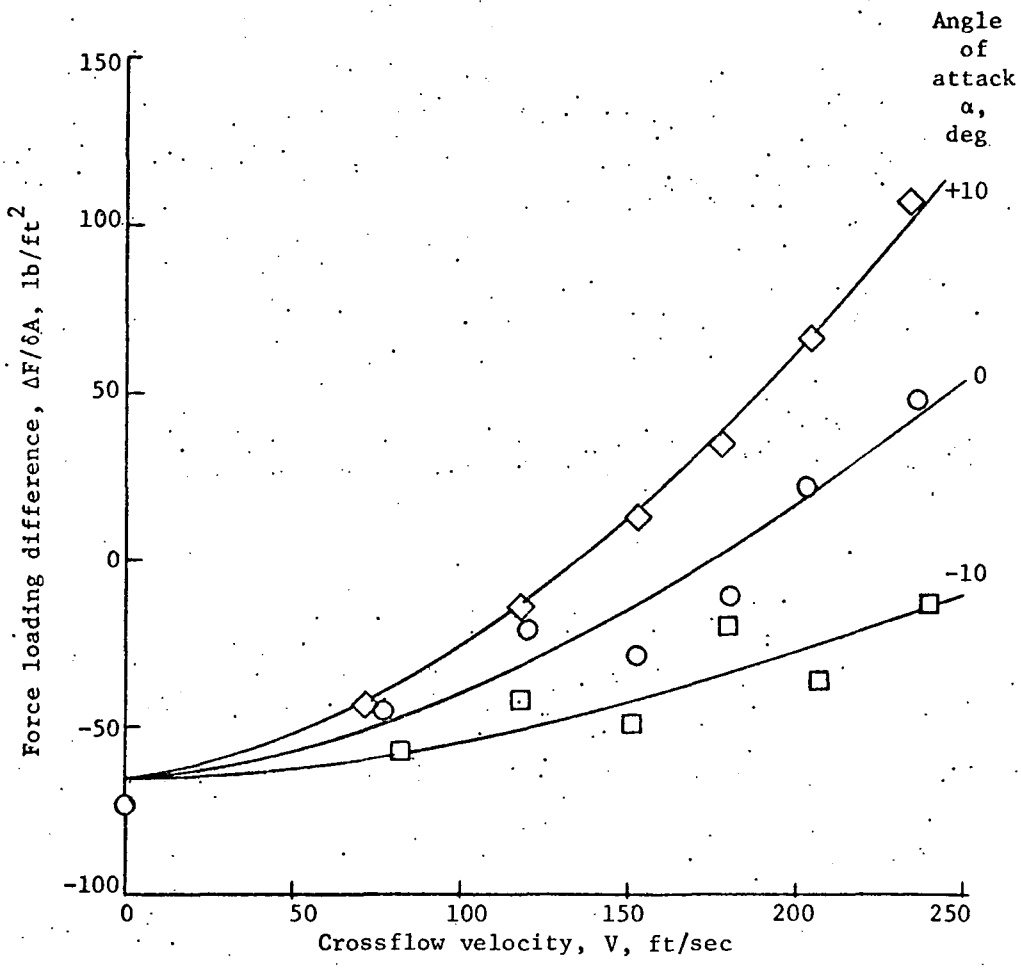

Figure 13. - Comparison of Computed Values from Correlation Equation and Observed Values of Force Loading Difference at 100 Percent of Design Speed.

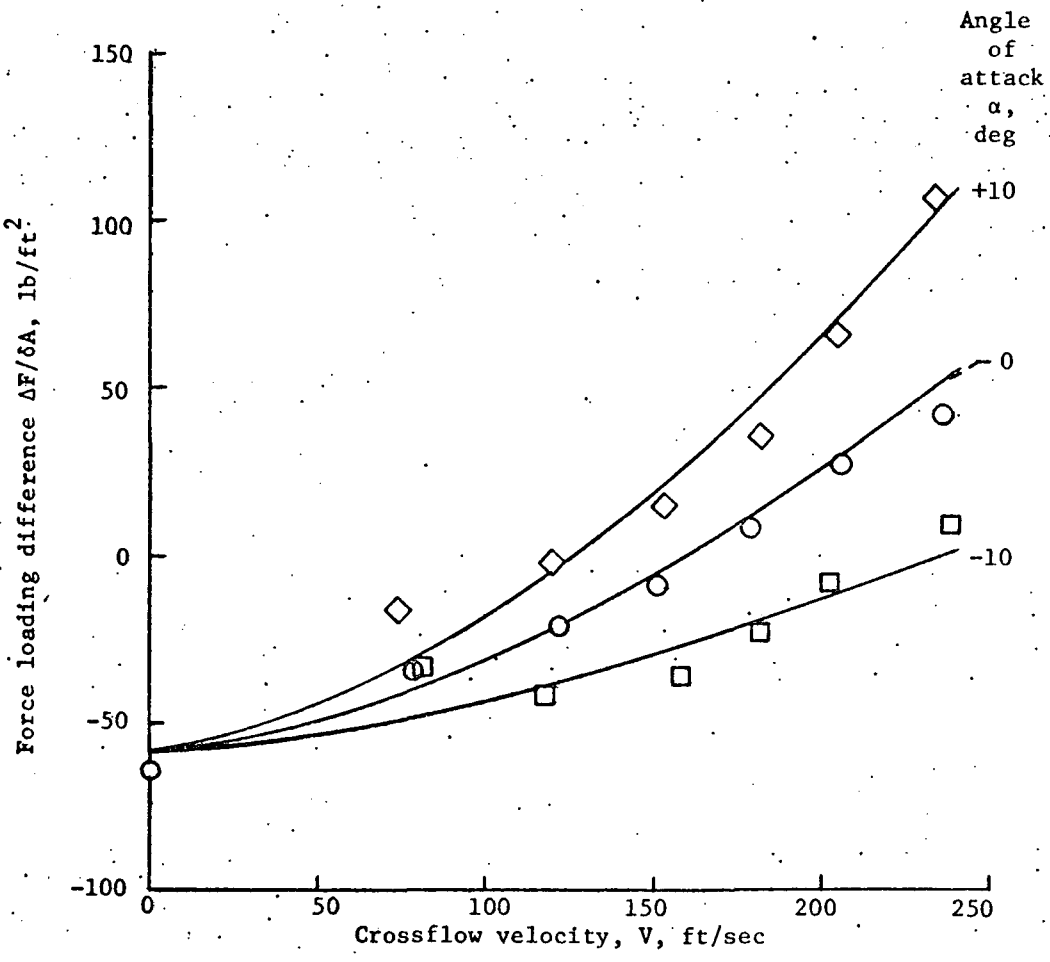

Figure 14. - Comparison of Computed Values from Correlation Equation and Observed Values of Force Loading Difference at 70 Percent of Design Speed.

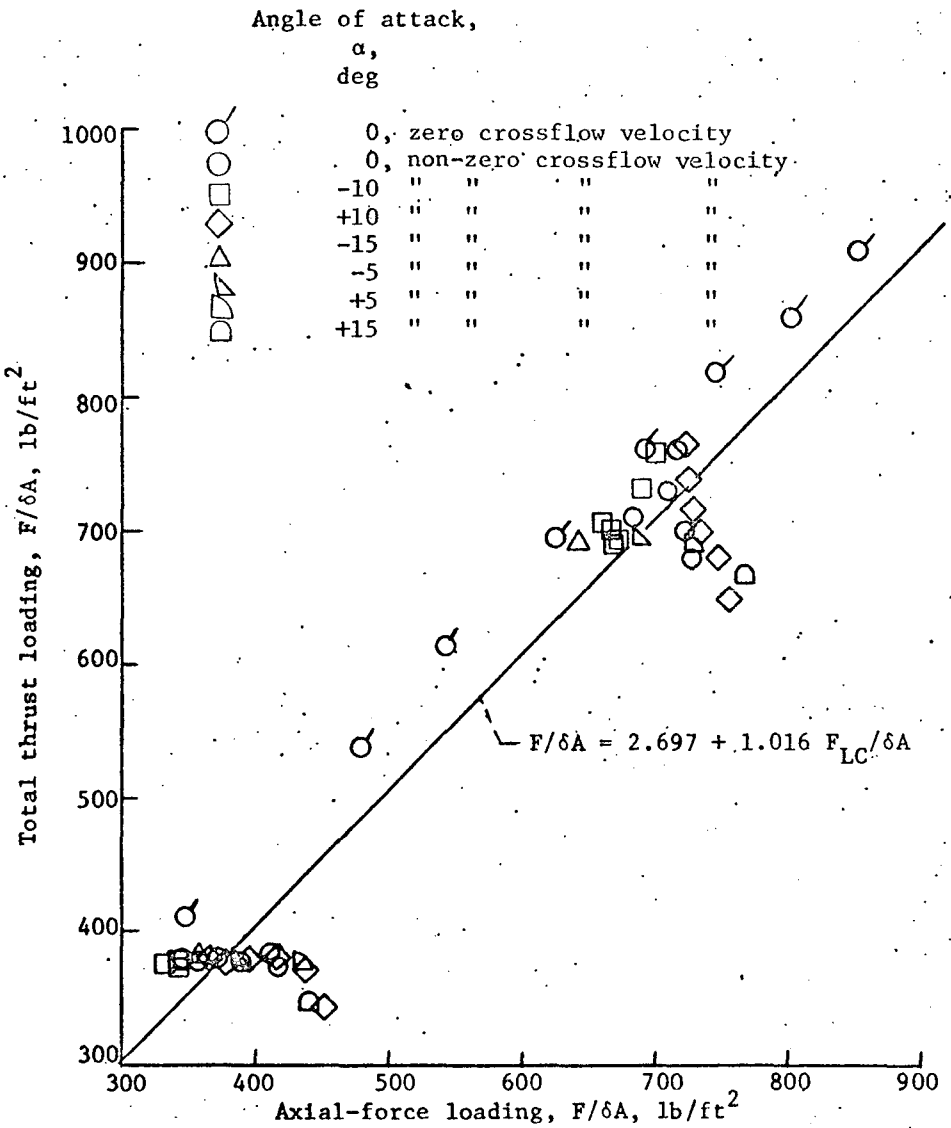

Figure 15. - Comparison of Correlation Equation and Observed Data for Total Thrust Loading as a Function of Axial-Force Loading.

crossflow velocity is to vary the observed data from the linear correlation equation shown. Further examination of the data on Figure 15 indicates that a family of lines with the same slope as the original correlation equation could be drawn through the data to represent constant values of angle of attack or crossflow velocity. The displacement of the lines from the original correlation equation would vary with crossflow velocity and angle of attack. It may then be possible to determine correlation equations for the family of lines to define the performance characteristics of the lift-fan simulator for the full range of dependent variables.

6.0 CONCLUSIONS AND AREAS FOR FURTHER RESEARCH

From the results of this experiment, the following major conclusions were reached:

The multiple linear regression analysis technique may be used to obtain significant correlation equations for the dependent variables: total thrust loading, axial-force loading, and the force loading difference as a function of the independent test variables: crossflow velocity, corrected tip speed, and wing angle of attack. The results of the multiple linear regression analysis showed that for all cases the correlation coefficient exceeded 0.988 which indicates a near perfect correlation. The F values obtained from the F-test for testing the null hypothesis H_0: that there is no correlation, were greater than the critical value of the F-distributions for a 0.01 probability level. Therefore, the null hypothesis H_0: that there is no correlation, was rejected and the alternative hypothesis H_1: that there is a significant correlation, was accepted.

The results of the linear regression analysis also showed that there is a significant correlation for the total thrust loading as a function of axial-force loading.

Since the linear regression analysis technique can calculate reliable prediction model equations, it would be possible to reduce the amount of instrumentation required to measure lift-fan simulator performance. For example, only a load cell force balance and

limited pressure instrumentation would be used to measure the lift-fan axial force, and the prediction model equation would then be used to calculate the total thrust load. Or if the lift-fan simulator design could not accommodate a force balance, the prediction model equation could be used to calculate the axial-force loading.

The prediction model equation was also useful in determining the relationship between the axial-force loading and the calculated total thrust loading. Crossflow velocity was found to be the most significant variable in the force-loading difference correlation equation. The correlation equations were also used to smooth the observed data. Smoothing the data helps to visualize the interference effects of the fan flow and external airflow (crossflow velocity) on the lift-fan simulator performance. It also helps to explain the reasons for the differences between the axial-force loading and the total thrust loading.

The experimental test results showed that the total thrust loading decreased uniformly with increasing crossflow velocity because of inlet flow separation and flow distortion effects on the exit total pressure. The axial-force loading tended to first decrease slightly and then increase with increasing crossflow velocity. This effect is a result of the combination of decreasing total thrust loading and increasing circulation pressure forces as the crossflow velocity increases.

The results of this work indicate that prediction modeling techniques could be valuable in designing and analyzing lift-fan

simulator tests. It could be used to reduce the amount of instrumentation required and to reduce the number of test runs required to define the performance characteristics of lift-fan simulators. The use of this technique could reduce the cost of building and testing lift-fan simulators.

However, a large amount of work remains to be done before the method presented in this thesis could actually be used routinely for any VTOL lift-fan test programs. The technique would have to be applied to other lift-fan simulator test programs to confirm the findings of this work. As previously stated, three other lift-fan simulator tests have recently been completed. This technique may also be applied to the results of those lift-fan simulator tests.

In addition, the techniques presented here should be applied to the test results of the lift-fan simulator tests with the exit louvers installed at the exit of the fan. The effect of exit louvers on the fan performance characteristics of the lift-fan simulator is a fourth independent variable to be included in the correlation equation.

The goal of this thesis was to develop a prediction technique to help in determining the performance characteristics of lift-fan simulators. The technique has tremendous potential, and it is hoped that this work will be a useful tool in the design and analysis of future lift-fan simulator test programs.

REFERENCES

1. Anon: Conference on V/STOL and STOL Aircraft. NASA SP-116, 1966, pp. 311-407.

2. Jagger, D. H.; and Kemp, E. D. G.: "The Potential and Development of a V/STOL Inter-City Airliner." Aircraft Eng., vol. 42, no. 1, Jan. 1970, pp. 6-13.

3. Deckert, Wallance H.; and Hickey, David H.: "Summary and Analysis of Feasibility-Study Designs of V/STOL Transport Aircraft." J. Aircraft, vol. 7, no. 1, Jan.-Feb. 1970, pp. 66-72.

4. Brown, D. G.: The Case for V/STOL Aircraft in Short-Haul Transportation. Paper 700333, SAE, April 1970.

5. Lieblein, S.: A Review of Lift Fan Propulsion Systems for Civil VTOL Transports. Paper 70-670, AIAA, June 1970.

6. Hickey, David H.: Preliminary Investigation of the Characteristics of a Two-Dimensional Wing and Propeller With the Propeller Plane of Rotation in the Wing-Chord Plane. NACA RM A57F03, 1957.

7. Hickey, David H.; and Ellis, David R.: Wind-Tunnel Tests of a Semispan Wing With a Fan Rotating in the Plane of the Wing. NASA TN D-88, 1959.

8. Wardlaw, R. L.; and Templin, R. J.: Preliminary Wind Tunnel Tests of a Lifting Fan in a Two-Dimensional Aerofoil. NAE Laboratory Report LR-207, 1957.

9. Wardlaw, R. L.; and McEachern, N. V.: A Wing-Submerged Lifting Fan: Wind Tunnel Investigations and Analysis of Transition Performance. NAE Laboratory Report LR-243, 1959.

10. Gregory, N.; and Raymer, W. G.: Wind Tunnel Tests on the Boulton Paul Rectangular Wing (Aspect Ratio 2) With Lifting Fan - Series I. A.R.C. 20,356 - F.M. 2717 - Perf 1692 - S. & C. 3299 - P.L. 17 - E.A. 710, 1958.

11. Gregory, M. A.; Raymer, W. G.; and Love, Edna M.: Wind Tunnel Test of a Wing Fitted With a Single Lifting Fan. N.P.L. Aero. Report 1129, 1964.

12. Hacket, J. E.: The Effect of Forward Speed on the Lift Produced by a Lifting Fan and Its Inlet. N.P.L. Report 1170, 1965.

13. Gregory, M. A.; Raymer, W. G.; and Love, Edna M.: The Effect of Forward Speed on the Inlet Flow Distribution and Performance of a Lifting Fan Installed in a Wing. R. & M. No. 3388, 1965.

14. Schaub, U. W.; and Bassett, R. W.: Analysis of the Performance of a Highly Loaded 12-Inch VTOL Z-Axis Fan-In-Wing Model at Zero Forward Speed. National Research Council of Canada Aeronautical Report LR-439, 1965.

15. Hickey, David H.; and Hall, Leo P.: Aerodynamic Characteristics of a Large-Scale Model with Two High Disk-Loading Fans Mounted in the Wing. NASA TN D-1650, 1963.

16. Hickey, D. H.; and Goldsmith, R. H.: Characteristics of Aircraft with Lifting-Fan Propulsion Systems for V/STOL. Institute of Aeronautical Sciences Paper 63-27. IAS 31st Meeting, N.Y., N.Y., Jan. 21-23, 1963.

17. Mort, Kenneth W.; and Yaggy, Paul F.: Aerodynamic Characteristics of a 4-Foot Diameter Ducted Fan Mounted on the Tip of a Semispan Wing. NASA TN D-1301, 1962.

18. Spreeman, Kenneth P.: Induced Interference Effects on Jet and Buried-Fan VTOL Configurations in Transition. NASA Conference on V/STOL Aircraft, 1960.

19. Norland, Sven-Anders: "An Investigation of the Lift Produced by a Fan in a Two-Dimensional Wing." Journal of American Helicopter Society, Vol. 7, No. 4, Oct. 1962.

20. Yuska, Joseph A.; and Diedrich, James H.; and Clough, Nestor: Lewis 9-by-15 Foot V/STOL Wind Tunnel. NASA TM X-2305, 1971.

21. Yuska, Joseph A.; and Diedrich, James H.: Fan and Wing Force Data From Wind-Tunnel Investigation of a 0.38 Meter (15-in.) Diameter VTOL Model Lift Fan Installed in a Two-Dimensional Wing. NASA TN D-6654, 1972.

22. Stockman, Norbert O.: "Potential Flow Solutions for Inlet of VTOL Lift Fans and Engines," Analytic Methods in Aircraft Aerodynamics, SP-228, 1969, NASA, Washington, D.C., pp. 659-681.

23. Moffitt, Thomas P.: Design and Experimental Investigation of a Single-Stage Turbine With a Rotor Entering Relative Mach Number of 2. NACA RM E58F20a, 1958.

24. Moffitt, Thomas P.; and Klag, Fredrick, W., Jr.: Experimental Investigation of Partial- and Full-Admission Characteristics of a Two-Stage Velocity-Compounded Turbine. NASA TM X-410, 1960.

25. Dudzinski, Thomas J.; and Krause, Lloyd N.: Flow-Direction Measurement With Fixed-Position Probes. NASA TM X-1904, 1969.

26. Staff of Lewis Laboratory: Central Automatic Data Processing System. NACA TN 4212, 1958.

27. Sidik, Steven M.; and Henry, Bert: RAPIER-A FORTRAN IV Program for Multiple Linear Regression Analysis Providing Internally Evaluated Remodeling. NASA TN D-5656, 1970.

28. Volk, William: Applied Statistics for Engineers, pp. 164-165. McGraw-Hill Book Company, New York, 1969.

APPENDIX A

METHOD OF CALCULATING TOTAL THRUST

This chapter describes the methods used in calculating the fan and turbine momentum thrust, axial force, and fan base force from the measured state point values of pressure, temperature and airflow angles, and axial force recorded at the various test points.

A.1 Momentum Thrust

The fan and turbine momentum thrust are calculated by the same procedure. The momentum thrust is calculated from the measured weight flow, and the ideal exit axial velocity calculated from the ideal expansion from a calculated total pressure to an undisturbed ambient pressure in conjunction with a thrust coefficient for outlet duct losses.

Fan Momentum Thrust. - The equation for the fan momentum thrust is

$$F_F = \frac{\dot{w}_1 V_{ze} C_{tf}}{g}, \text{ lb} \qquad \text{(A1)}$$

where C_{tf} is the thrust coefficient determined from experimental data of similar exit ducts. For this application C_t 1.0. The acceleration due to gravity, g = 32.2 ft/sec^2. V_{ze} is the ideal exit axial velocity and is determined from the following equation.

$$V_{ze} = \cos \bar{\beta}_e \left\{ 2g \left(\frac{\gamma}{\gamma - 1} \right) \hat{T}_e \left[1 - \frac{p_o}{\hat{P}_e} \right]^{\frac{\gamma-1}{\gamma}} \right\}^{1/2}, \text{ ft/sec} \qquad \text{(A2)}$$

where p_o is the undisturbed ambient static pressure measured in the test section, $\hat{P}_e$ is the average total pressure at the fan exit weighted according to the distribution of mass flow in the fan passage (such terms are denoted as mass averaged terms); $\bar{\beta}_e$ is the average airflow angle; $\hat{T}_e$ is the mass averaged total temperature, and γ is the ratio of specific heat of air, $\gamma = 1.4$.

The weight flow $\dot{w}_1$ is calculated from the correlation

$$\dot{w}_1\sqrt{\theta}/\delta \doteq f(p_1/p_o), \text{ lb/sec} \tag{A3}$$

where p_1 is the fan inlet static pressure 3/4 of an inch above the rotor leading edge. The correlation is obtained from a computer program based on the potential flow theory of reference 22 for an inlet sufficiently far upstream of the rotor to be considered unaffected by the rotor. The weight flow is also adjusted for the effects of flow separation on the inlet bellmouth.

Turbine Momentum Thrust. - The equation for turbine momentum thrust is

$$F_T = \frac{\dot{w}_T V_{zT} C_{tf}}{g}, \text{ lb} \tag{A4}$$

where the thrust coefficient $C_{tf} = 0.98$. V_{zT} is the ideal exit axial velocity and is determined from the following equation.

$$V_{zT} = \cos \bar{\beta}_T \left\{ 2g \left(\frac{\gamma}{\gamma - 1} \right) \hat{T}_T \left[1 - \left(\frac{p_o}{P_T} \right)^{\frac{\gamma-1}{\gamma}} \right] \right\}^{1/2}, \text{ ft/sec} \tag{A5}$$

Where $\hat{P}_T$ is the mass averaged total pressure at the turbine exit, $\hat{T}_T$ is the mass averaged total temperature, and $\bar{\beta}_T$ is the average airflow angle. The weight flow $\dot{w}_T$ is measured with a calibrated flat-plate orifice.

A.2 Fan Base Force

The fan base force F_B is calculated from the measured static pressure p_b acting on the lower surface of the fan hub.

$$F_B = (p_o - p_b)A_b, \text{ lb} \qquad \text{(A6)}$$

Where p_o is the ambient static pressure in the test section, and A_b is the area on which p_b acts ($A_b = 0.227$ ft^2 for this experiment).

A.3 Axial Force

The axial force is measured on the load cell force balance. The force balance consists of three 500 lb load cells equally spaced on a 22.5-in. diameter circle (Fig. 3). The total axial force is the sum of the three load cell readings times a calibration constant

$$F_{LC} = (F_1 + F_2 + F_3)K_f, \text{ lb.} \qquad \text{(A7)}$$

where F_1, F_2, and F_3 are the individual load cell readings. K_f is a calibration constant determined from calibration tests of the load cell force balance.

APPENDIX B

DESCRIPTION OF MULTIPLE LINEAR REGRESSION COMPUTER PROGRAM

RAPIER[27] is a FORTRAN IV program for multiple linear regression analysis. RAPIER computes the variance-convariance matrix of the independent variables, regression coefficients, t-statistics for individual tests, and analysis of variance tables for overall testing of regression. There is a choice of three strategies for the variance estimate to be used in computing t-statistics. A backward rejection option method, based on the first dependent variable, may be used. A critical significance level is supplied as input. The least significant independent variable is deleted and the regression recomputed. This process is repeated until all remaining variables have significantly nonzero coefficients.

The model equation is assumed to be of the form

$$y_i = b_1 x_{i_1} + b_2 x_{i_2} + \cdots + b_J x_{iJ} + e_i \qquad i = 1,\ldots N \qquad (B1)$$

where:

y_i is the response variable.

x_{iJ} is the transformation of the independent variables. The subscript i indicates the values associated with the i^{th} observation.

The subscript J denotes the number of independent variables observed.

N is the number of observations.

e_i denotes the difference between the observed value and the expected value of y_i.

The program then computes the regression coefficients b_0, b_1,.... b_9; the (Analysis of Variance) ANOVA table; the coefficient of determination r^2, and the coefficient of correlation r; the standard error of the regression estimate. In addition an F test is made for testing the null hypothesis H_0: that there is no correlation, that all the correlation coefficients are zero, the alternative hypothesis is H_1: that there is a significant correlation. The F test is

$$F = \frac{\text{Mean squares of the regression}}{\text{Mean squares of the residual}}$$

If the calculated value of F is greater than the critical value of the F distributions for the number of degrees of freedom, then the hypothesis H_0 is invalid indicating that there is a significant correlation and the regression coefficients are not zero.

If the backward rejection option of the program is used a t-test is performed on each regression coefficient. The term corresponding to the minimum t is dropped and the regression is recomputed. This process is repeated until all remaining coefficients are significant at the specified level of confidence.

Then for each observation (input data) the observed response (y), the calculated response (y calc); the residual (Y obs - Y calc = Diff), and the studentized residual $z = \frac{y - \bar{y}}{\hat{\sigma}}$ is computed and printed out. Two other statistics which may be used to test the normality of the empirical distribution, skewness and kurtosis, are calculated. Skewness should be nearly zero and kurtosis should be nearly 3.

The program has a prediction option, in which the regression equations are used to predict an estimated response at some condition of the independent variables. The program accepts input vectors x and computes the predicted response, y; the variance of the regression line, the standard deviation of regression, variance of the predicted value and the standard deviation of the predicted value.

The program also has a computer plot routine which plots the residuals for the dependent variable versus the independent variables and the residuals for the dependent variable versus the predicted value.

APPENDIX C

GLOSSARY OF SYMBOLS

A	fan frontal area, 1.263 ft^2
A_b	fan hub base area, 0.227 ft^2
b_i	regression coefficient
C_{tf}	thrust coefficient
F	total thrust force, lb
F_B	fan base force, lb
F_F	fan momentum thrust, lb
F_i	individual load cell reading, lb
F_{LC}	axial-force measured on load cell force balance, lb
F_T	turbine momentum thrust, lb
$F/\delta A$	total thrust loading parameter, lb/ft^2
$F_{LC}/\delta A$	axial-force loading parameter, lb/ft^2
$\Delta F/\delta A$	force loading difference, lb/ft^2
H_0	statistical hypothesis to be tested
H_1	alternative hypothesis to be accepted if H_0 is judged to be false
P	total pressure measurement, lb/ft^2
P_A	total pressure measurement for airflow angle, lb/ft^2
$\hat{P}_e$	mass averaged fan exit total pressure, lb/ft^2
P_b	static pressure on lower surface of fan hub, lb/ft^2
P_s	static pressure measurement, lb/ft^2
p_1	fan inlet static pressure, lb/ft^2
ΔP	differential pressure measurement, lb/ft^2

T	total temperature measurement, ^{o}R
$\hat{T}_e$	mass averaged fan exit total temperature, ^{o}R
$\hat{T}_T$	mass averaged turbine exit total temperature, ^{o}R
ΔT	differential total temperature measurement, ^{o}R
$U_T/\sqrt{\theta}$	fan corrected tip speed, ft/sec
V	crossflow velocity (free stream airflow), ft/sec
V_{ze}	ideal exit axial velocity of fan, ft/sec
V_{zT}	ideal exit axial velocity of turbine, ft/sec
$\dot{w}_1$	fan weight flow, lb/sec
$\dot{w}_T$	turbine weight flow, lb/sec
y	dependent variable for regression analysis
α	wing angle of attack, deg
β	airflow angle, deg
δ	the ratio of inlet total pressure to standard sea-level pressure of 2116.2 lb/ft^2
θ	the ratio of inlet total pressure to standard sea-level temperature 518.7^{o} R
γ	ratio of the specific heat of air, $\gamma = 1.4$